iScience

CellPress
OPEN ACCESS

Article

Assessment of drug permeability through an ex vivo porcine round window membrane model

Adele Moatti,
Dylan Silkstone,
Taylor Martin, ...,
Alan G Cheng,
Frances S Ligler,
Alon Greenbaum

greenbaum@ncsu.edu

Highlights

The porcine round window membrane (RWM) mimics the human RWM in structure and thickness

The porcine RWM model, extracted from fresh tissue, remains viable for up to five days

Drug passage and permeability can be measured at multiple time points via the RWM model

The RWM model is a valued tool for testing techniques aimed at enhancing RWM permeability

Moatti et al., iScience *26*, 106789
June 16, 2023
https://doi.org/10.1016/j.isci.2023.106789

iScience

CellPress
OPEN ACCESS

Article

Assessment of drug permeability through an ex vivo porcine round window membrane model

Adele Moatti,[1,2] Dylan Silkstone,[1,2] Taylor Martin,[2,3] Keith Abbey,[1] Kendall A Hutson,[4] Douglas C Fitzpatrick,[4] Carlton J Zdanski,[4] Alan G Cheng,[5] Frances S Ligler,[6] and Alon Greenbaum[1,2,7,*]

SUMMARY

Delivery of pharmaceutical therapeutics to the inner ear to treat and prevent hearing loss is challenging. Systemic delivery is not effective as only a small fraction of the therapeutic agent reaches the inner ear. Invasive surgeries to inject through the round window membrane (RWM) or cochleostomy may cause damage to the inner ear. An alternative approach is to administer drugs into the middle ear using an intratympanic injection, with the drugs primarily passing through the RWM to the inner ear. However, the RWM is a barrier, only permeable to a small number of molecules. To study and enhance the RWM permeability, we developed an *ex vivo* porcine RWM model, similar in structure and thickness to the human RWM. The model is viable for days, and drug passage can be measured at multiple time points. This model provides a straightforward approach to developing effective and non-invasive delivery methods to the inner ear.

INTRODUCTION

Hearing loss affects nearly 20% of the global population,[1] and recently several studies linked hearing loss to cognitive declines, such as increasing rate of dementia, Parkinson's disease, and depression.[2–4] To mitigate the detrimental effects of hearing loss, hearing aids and cochlear implants are commonly used, with limited success. Not only may some cochlear implant users lose their residual low-frequency hearing, but they also cannot discriminate speech or attend to a specific source of sound within the noisy environment. Hearing aid users also suffer from a lack of normal auditory perception.[5–7] Consequently, many researchers are seeking to develop alternative treatments to restore hearing or prevent hearing loss. A major obstacle to translating these novel treatments to patients is the lack of effective and minimally invasive procedures to deliver substances to the inner ear.[8] Systemic delivery is challenging as only a fraction of the injected therapeutic agent passes through the blood labyrinth barrier and reaches the inner ear.[8] Local delivery via intracochlear and intra-round window membrane (RWM) procedures seems promising, but these procedures have major shortcomings including increased risk for hearing loss through cerebrospinal and perilymph fluid leakage and exhibiting large variability in the therapeutic outcomes.[9,10] The intratympanic injection method is less invasive and causes minimal damage to the inner ear; it is also used clinically to deliver steroids such as dexamethasone (Dex) and gentamicin to treat idiopathic sudden sensorineural hearing loss and Menière's disease.[11–17] However, since the injected substances that fill the middle ear cavity must pass through the RWM, intratympanic injection is less effective in delivering substances with large molecular weight, negative change, or hydrophilic properties to the inner ear.[18]

The RWM is an epithelial barrier that consists of three layers. The first and outer layer, facing the middle ear, consists of epithelial cuboidal cells that form tight junctions. The tight junctions prevent the passage of most molecules via passive diffusion. The second layer is made of fibroblasts, collagen, and elastic fibers,[19] and contains blood and lymph vessels as well as nerve endings. The third layer consists of squamous flat inner epithelial cells, facing the scala tympani (Figures 1A and 1B). To improve the permeability of substances to the RWM, methods such as partial digestion and permeabilization of the RWM,[20,21] ultrasound microbubble disruption,[22] and the creation of a micro-perforations[23] have been tested in animals. Most of these experiments were performed *in vivo*, with only limited temporal sampling points, and conducted in rodent models that do not mimic their human counterparts in terms of RWM thickness (~10–15 μm in rodents compared to 70 μm in humans).[18,24–28] Therefore, there is a need for a physiologically

[1]Joint Department of Biomedical Engineering, University of North Carolina at Chapel Hill and North Carolina State University, Raleigh, NC 27606, USA

[2]Comparative Medicine Institute, North Carolina State University, Raleigh, NC 27606, USA

[3]Department of Chemical and Biomolecular Engineering, North Carolina State University, Raleigh, NC 27606, USA

[4]Department of Otolaryngology- Head and Neck Surgery, University of North Carolina at Chapel Hill, Chapel Hill, NC 27599, USA

[5]Department of Otolaryngology-Head and Neck Surgery, Stanford University, Stanford, CA 94305, USA

[6]Department of Biomedical Engineering, Texas A&M University, College Station, TX 77843, USA

[7]Lead contact

*Correspondence: greenbaum@ncsu.edu

https://doi.org/10.1016/j.isci.2023.106789

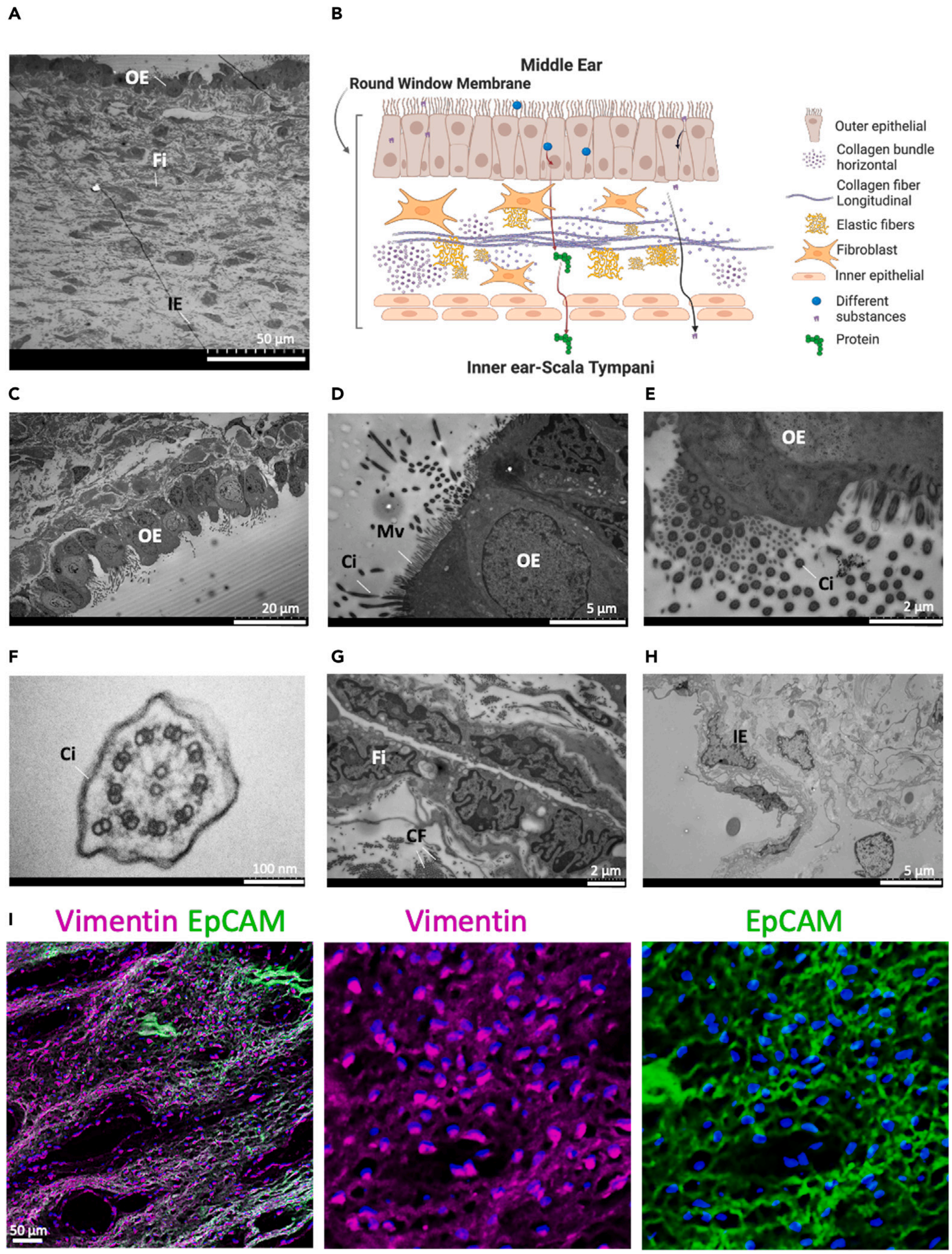

Figure 1. The microstructure and cellular constitution of the porcine RWM

(A) A TEM micrograph of the porcine RWM that shows three layers structure that consists of the outer epithelial (OE) layer, fibroblast (Fi) layer, and inner epithelial (IE) layer.

(B) A schematic of the porcine RWM that shows a three-layered structure corresponding to (a) that consists of the OE layer, Fi layer, and IE layer. In the fibroblast layer collagen fibers (CFs) and elastic fibers (EFs) can be observed.

(C) A TEM micrograph that shows that the porcine OE cells form tight junctions that can restrict the passage of molecules. Using TEM, microvilli (Mv) and cilia (Ci) can be observed on the edges of the OE cells.

(D–F). The cilia in (f) present the canonical 9 + 2 structure.

(G) A TEM micrograph of the fibroblast cells and the collagen fibers in their vicinity.

(H) A TEM micrograph of the IE layer, which includes squamous epithelial cells.

(I) Immunostaining of the porcine RWM using epithelial (anti-EpCAM or CD326) and fibroblast (anti-Vimentin) cell markers shows the presence of the two cell types in the porcine RWM. See Figure S1.

relevant *ex vivo* RWM model to easily test and explore innovative delivery methods to the inner ear across multiple time points.

Few attempts have been made to generate an RWM model in small animal models due to the difficulty of accessing and excising the RWM. Some of the early RWM models used RWM tissues from guinea pigs to reconstruct a chamber with two cavities resembling the middle and the inner ear.[29–31] In a more recent study, guinea pig RWM was dissected, attached to a membranous sheet, and inserted in a Vertical Franz Diffusion Cell™.[23] These aforementioned models provide interesting platforms, but the studies were conducted with rodent RWM, which is five to six times thinner than the human RWM[18,25–28]; thus, the reported values for passage across the RWM are not directly translational. More importantly, none of these studies monitored tissue viability, and in our hands, the permeability of the RWM is proportional to explant tissue death. In the absence of a viable *ex vivo* RWM with dimensions comparable to that of humans, the realization of rules governing the transport of small molecules, macromolecules, and viruses across the RWM and testing innovative therapies to address hearing loss will remain difficult.

In this study, we developed and tested an easy-to-build *ex vivo* porcine RWM model. The porcine RWM has a similar thickness to human RWM, and given its large size, the porcine RWM is comparatively easy to excise and handle. Using this RWM model, we evaluated the passage of the non-salt form of Dex, known to be highly permeable across the RWM, and the low-permeability non-salt form of Dex conjugated with fluorescein (DexF) as a function of cell viability over a course of 24 h. We then evaluated the effect of permeabilization of the RWM on DexF passage using saponin and collagenase, which have been shown to improve permeability *in vivo* in small animal models.[20] Our *ex vivo* model can serve as an effective testing chamber to study the passage of substances through the RWM to the inner ear and to test much-needed approaches to improve delivery methods to the inner ear.

RESULTS

Investigation of the porcine RWM properties using transmission electron microscopy and immunohistochemistry

As a first step in creating the porcine *ex vivo* RWM model, we characterized the porcine RWM using transmission electron microscopy (TEM; Figures 1C–1H) and immunohistochemistry (IHC; Figure 1I). The RWM structure revealed that the RWM consists of three layers with two epithelia and a middle mesodermal connective tissue layer (Figure 1A). This three-layered structure agrees with the literature[25] and is depicted in Figure 1B. The outer epithelial (OE) cuboidal cells that sit in the vicinity of the middle ear cavity form tight junctions, shown in Figure S1A, that restrict the passage of molecules from the middle to the inner ear (Figures 1C–1E). These cells are active and have mitochondria (Mi) and rough and smooth endoplasmic reticulum (RER and SER) as shown in Figure S1A. We also observed OE cells with short microvilli (Mv) and cilia (Ci), which may facilitate absorption or move particles away from the epithelial barrier. The cilia contain a 9 + 2 arrangement of microtubules (Figures 1D–1F). The 9 + 2 arrangement refers to how the microtubules are organized; it has 9 fused pairs arranged on the outside and 2 unfused pairs in the center. The cilia might be present to move particles away from the epithelial barrier. The middle layer consists of fibroblastic (Fi) and collagen fibers (CFs) (Figure 1G). We have also observed a node of Ranvier structure in the RWM middle layer that indicates the rapid traveling of the action potential along the fibers through the RWM (Figure S1B). The inner layer includes the squamous inner epithelia (IEs) with loose junctions (Figure 1H). To verify the presence of epithelial cells and fibroblasts in the porcine RWM, we used IHC (Figure 1I). As shown in the higher-resolution images, the antibodies unveiled the cuboidal shapes of the epithelial cells and elongated shapes of the fibroblasts. The presence of wrinkles is due to the detachment of the membrane from the bony structure.

As the next step of our experiment, we measured the thickness of the porcine RWM, stained with DAPI (4′,6-diamidino-2-phenylindole, a blue-fluorescent DNA stain) and anti-EpCAM (epithelial cellular adhesion molecule, CD326), using confocal microscopy (Figures S1C and S1D). We measured the RWM thickness since it is reported that the thickness is critical in defining the permeability of substances across the RWM.[25] We used H&E staining at different ages and observed different RWM thicknesses between post-natal day (P) 0 and P40 pigs (Figures S1E–S1F). The measured RWM thicknesses using H&E images for P0 and P40 pigs are 92 ± 16 and 136 ± 9 μm, respectively (three cross sections at various locations, mean $\pm$ SD). These measurements are not absolute and might vary at different locations on the RWM. All in all, we have found that the porcine RWM is more similar to the human RWM in anatomy and structure and therefore suitable to use as an *ex vivo* RWM model.

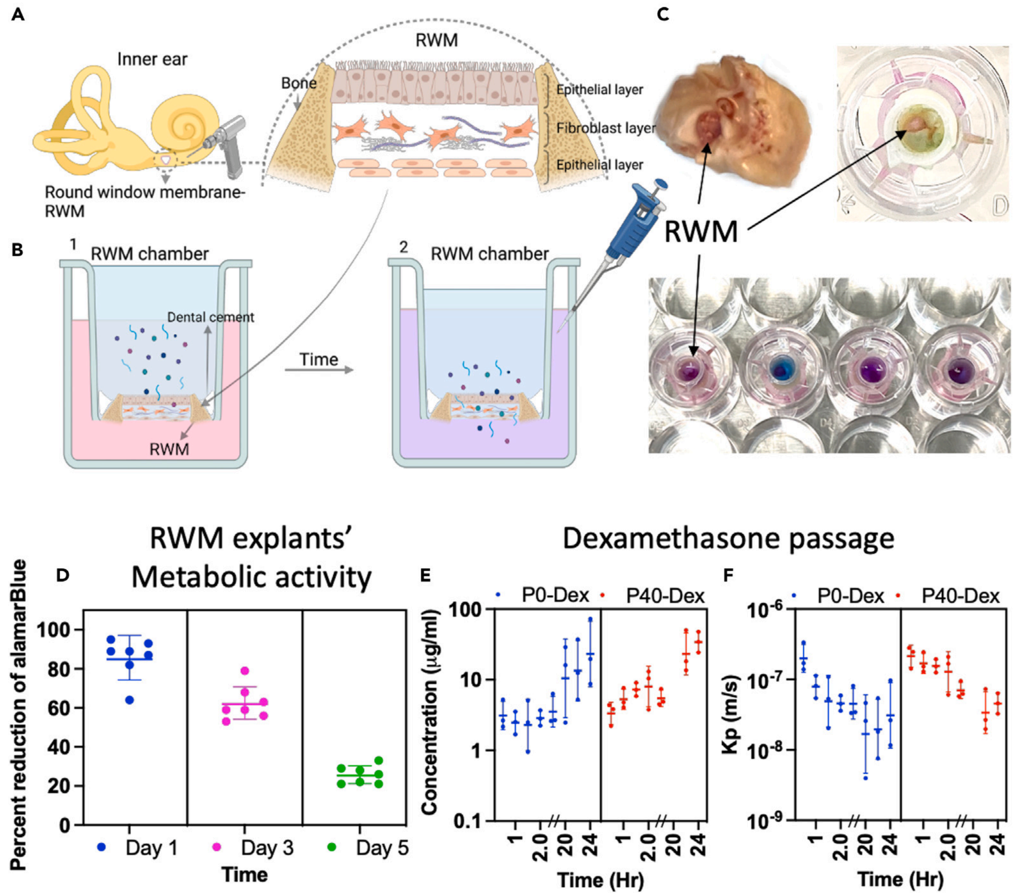

Figure 2. The porcine *ex vivo* RWM chamber

(A) In a schematic of the inner ear, the dashed circle marks the RWM location, which is excised using a dental drill.

(B) A schematic of the excised RWM with the three-layer structure and the surrounding bone inside a testing chamber separating the chamber into the top and bottom of the RWM that resembles middle and inner ear cavities, respectively.

(C) The real-life RWM chambers. The excised RWM inside a plate insert. The test substances were dropped into the top part of the chamber, and fluid beneath the RWM in the bottom part of the chamber was sampled at various time points. Photographs of the real-life post-natal day 0 (P0) porcine inner ear, the excised RWM that was inserted inside the testing chamber, and the testing substances on top of chambers.

(D) The results of the alamarBlue test for metabolic activity of RWM explants (n = 7) are reported as a percent reduction (mean $\pm$ SD). The innate metabolic activity of the cells inside the explants, as an indirect measure of viability, results in a chemical reduction of alamarBlue. This reduction causes the redox indicator to change from oxidized (non-fluorescent, blue) to reduced (fluorescent, red) form that can be detected by a plate reader. The higher the percent reduction is, the higher the metabolic activity of the cells in the explant is. The test is done over a period of 5 days, and at each measurement, the alamarBlue incubation period was 4 h hours.

(E) Dexamethasone ($\sim$400 μg/mL) passage through the RWM chamber over a period of 24 h starting on the second Day. Dexamethasone was redosed (10 μL) at each sampling point. The experiment was conducted on 3 P0 and 3 P40 porcine RWM explants (mean $\pm$ SD). The zero time point had a value of 0.058 μg/mL.

(F) The corresponding calculated permeability (K_p) of dexamethasone (mean $\pm$ SD) based on the measured concentrations in (e). The sampling points in e and f are 0.5, 1, 1.5, 2, 2.5, 20, 22, and 24 h. See Figure S2.

The *ex vivo* RWM chamber design, viability, and function

After establishing the characteristics of the porcine RWM, we designed a porcine *ex vivo* RWM chamber. Figures 2A–2C show the procedure for making the chamber. First, we dissected the porcine inner ear out of the pig skull.[32] Then, using a dental drill, we excised the RWM including the bony structure that supports it and mounted the excised tissue inside a transwell insert using a dental cement. When the insert is put into a chamber, the passage of substances can be tested (Figures 2B and 2C display the real-life P0 porcine inner ear and its RWM inside the working chambers).

We then examined the viability of the excised RWM explants over time. The viability of the RWM is critical as the absence of active processes and detachment of dead cells could possibly artificially increase the passage of substances. We utilized the alamarBlue metabolic activity assay to infer the cellular activity of the RWM explants and consequently their viability (Figure 2D). Note, the higher the percent reduction (PR), the higher the metabolic activity of the cells in the explant. The results are displayed in Figure 2D. We calculated the PR for 7 explants up to 5 days. As it is evident, the metabolic activity in the chamber decreased with time, and by day 5 it is only ~20%. Thus, we tested the passage of substances in the chamber for up to 3 days where explants show the highest viability.

To establish the functionality of our chamber, we tested the passage of a known high-permeability therapeutic, Dex, which has been shown to pass through the RWM in multiple animal models and humans.[17,27,30,33] We placed ~400 μg/mL Dex (1 mM) in a mixture of methanol: culture media (~1:25) on top of the six RWM chambers (3 P0 and 3 P40), and we analyzed the concentration at the bottom of the chamber using an ELISA (enzyme-linked immunoassay) kit. The results are depicted in Figure 2E. As expected, significant amounts of Dex passed through the RWM in 0.5 h (unpaired t-test, p value = 0.0024), with increasing amounts accumulating in the lower chamber over 24 h. We did not observe any differences between the sexes. We did not observe any significant difference in Dex passage through explants from different ages.

We have also calculated the permeability coefficient (K_P) of RWM to Dex at different time points and plotted it in Figure 2F. We calculated the average of the K_p at two different regimes of 0.5–2.5 h and 20-24 h to be 12.3 ± 4.6 e−8 m/s and 3.8 ± 2.4 e−8 m/s (mean ± SD), respectively.

Measuring the passage of a low-permeability substance through the *ex vivo* RWM

Next, we examined the passage of a larger molecule with lower permeability through the RWM explants—DexF. The difference between the molecular structures of Dex and DexF is shown schematically in Figure 3A. Based on the literature, we expected that DexF would exhibit a lower passage than Dex,[20] as shown in the schematic in Figure 3A. To test DexF passage, we placed ~500 μg/mL (0.5 mM) DexF in a mixture of methanol: culture media (1:1.37) on top of nine chambers containing RWMs from pigs of different ages (3 P0, 3 P20, and 3 P40; total n = 9). The media at the bottom of the chamber were collected and analyzed using a plate reader at multiple time points (Figure 3B). The DexF passed across the membrane less efficiently than Dex. We then calculated the K_p for all the explants at different time points as shown in Figure 3C. The average K_p values during 0.5–4.5 h and 20–24 h from the introduction of DexF are calculated respectively to be 6.2 ± 2.7 e−9 m/s and 5.4 ± 3.2 e−10 m/s for P0-P20 and 6.5 ± 3.2 e−10 m/s and 2.9 ± 0.2 e−10 m/s (mean ± SD) for P40. The measured K_p for DexF is found to be two orders of magnitude lower than that for Dex. Similar to Dex, the permeability of DexF decreases over time by one order of magnitude (Figure 3C). We also observed a significant decrease in the K_p of the P40 in comparison to P0-20 explants after 1 h, using a two-way ANOVA test (p value = 0.0121). The passage of fluorescein alone is shown in Figures S3A and S3B, which is significantly different from DexF only after 2.5 h (p value= 0.0011).

We also tested how longer times in the chamber affected the DexF passage, our assumption being that over time cells would die, and we assumed that dead cells compromised the structural integrity or influence active passage processes (e.g., exocytosis). We categorized the explants into three groups: 1) the healthy explants with 80–100% PR (high metabolic activity and viable), 2) the low-viability explants (low metabolic activity) where the PR is 15–30% but the RWM can support the fluid in the upper chamber for more than 3–4 h, and 3) the leaky explants that are highly viable but have microscopic defects such as holes (see Figure S4) and hold the solution for more than 3–4 h. Note that the viable leaky explants with micron-sized holes required a microscope and careful examination to observe the holes; these holes cannot be seen by the naked eye. These three groups are shown schematically in Figure 4A. Toward this end, we purposefully tested and compared the passage of DexF on four leaky explants (with microscopic defects) and on three low-viability explants compared to healthy and highly-viable (control) ones as shown in Figure 4B. We observed that the passage of DexF through the low-viability and leaky RWM was higher than that through healthy explants. The K_p values are shown in Figure 4C, and they were calculated for two time points (0.5–4.5 h from the introduction of DexF and 20–24 h): 5.0 ± 5.8 e−8 m/s and 1.3 ± 0.8 e−8 m/s for low-viability explants and 15.2 ± 4.4 e−8 m/s and 3.2 ± 1.7 e−8 m/s for leaky explants (mean ± SD). In comparison with the healthy chambers, both the leaky and the low-viability groups have K_p values that are two orders of magnitude higher. This result showed that the high viability of the RWM chamber was crucial for assessing the permeability of materials, which provided the basis for our exclusion criteria.

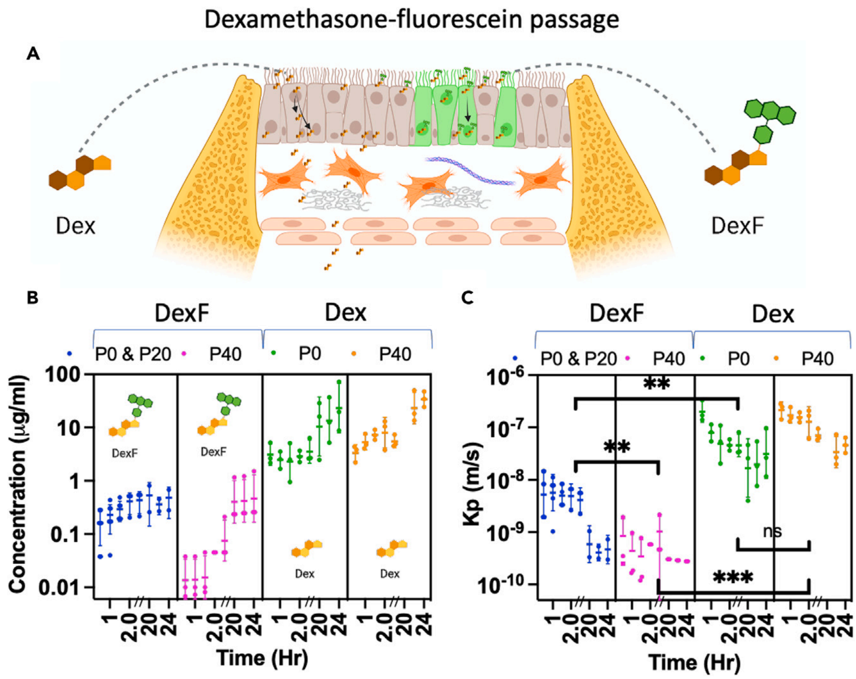

Figure 3. The porcine *ex vivo* RWM chamber shows relatively lower passage for low-permeability material

(A) A schematic of dexamethasone: Dex and dexamethasone-fluorescein: DexF structure and passage through the RWM is shown.

(B) Passage of ~500 μg/mL (0.5 mM) DexF and ~400 μg/mL (1 mM) Dex through the RWM chamber over a period of 24 h (mean ± SD). The experiments were conducted on n = 6 P0-P20 and n = 3 P40 porcine RWM explants for DexF and on n = 3 P0 and n = 3 P40 porcine RWM explants for Dex.

(C) The calculated permeability (K_p) of DexF and Dex (mean ± SD). A nested t-test was performed to show the significant differences with p = 0.0015 for P0&P20-DexF vs. P40-DexF passage, p = 0.0099 for P0&P20-Dex vs. P0-DexF passage, and p = 0.0001 for the difference between and P40-DexF vs. P40-Dex passage. The sampling points in b and c are 0.5, 1, 1.5, 2, 2.5, 20, 22, and 24 h. See Figure S3 and Video S1.

Assessing the passage dynamics and mechanism of DexF

To further investigate the mechanism of the passage through the RWM, we took advantage of the fluorescent properties of DexF and imaged the explants at several time points after adding DexF (0.5, 2.5, and 24 h). The results are shown in Figures 5A–5C. After 0.5 h (Figure 5A), we noticed only a few instances where fluorescence was present in the cell nucleus (Figure 5A), and in general, the sample showed a very low fluorescence background. After 2.5 h (Figure 5B), a strong fluorescence signal was observed in the cell nucleus, and surprisingly, after 24 h (Figure 5C), the fluorescence signal was mostly found in the cell cytoplasm and not in the nucleus. The proposed schematic of the DexF interaction with OE is described in Figure 5D. Also, we observed that the fluorescence intensity is limited to the top 30 μm of the RWM throughout the 24-h period (see Video S1, and Figure S3B). To investigate whether the DexF migration from the nucleus to the cytoplasm was limited to the pig, we used live-cell imaging of the OE cells of mouse RWM (Figures S5A and S5B) and observed similar behavior. In mice, the DexF is initially present in the cytoplasm and then slowly moves to the nucleus, and after about 3.5 h, the nucleus expresses no fluorescence signal.

We also confirmed that no fluorescent signal is present in the nucleus in the event that cells are dead when DexF was delivered in front of the RMW via intratympanic injection in cadaver pigs (Figure S6).

The effects of collagenase and saponin treatment on RWM permeability

Several studies have treated the RWM with enzymes and compounds[20,21] to enhance the drug passage through the RWM of rodents. We tested whether these treatments are also effective on the thicker porcine RWM.

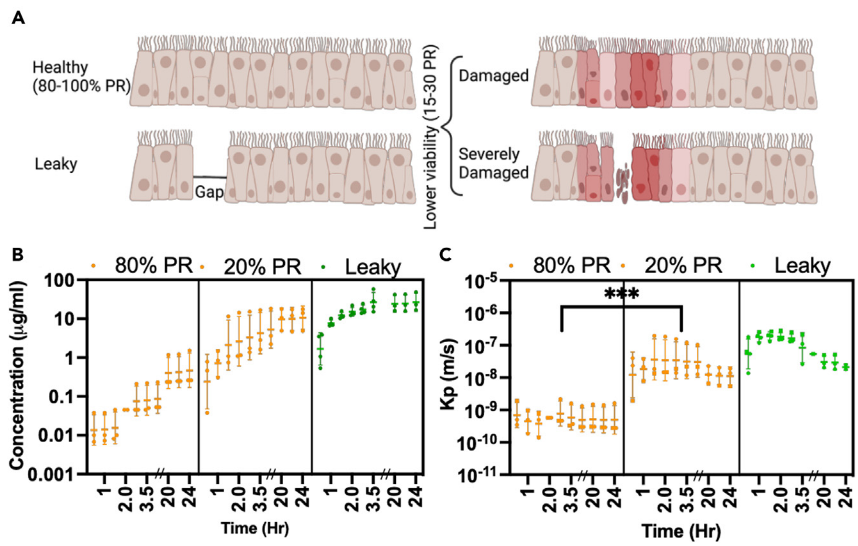

Figure 4. The *ex vivo* chamber viability is critical to assess permeability

(A) A schematic that shows the differences in the RWM structure between healthy (80–100% Percent reduction: PR), leaky, but healthy, (including microscopic holes or tears), and low-viability (15–30% PR) explants.

(B) Passage of ~500 μg/mL (0.5 mM) DexF was tested over a period of 24 h on n = 3 healthy (80–100% PR), n = 3 low-viability, and n = 4 leaky porcine RWM explants (mean ± SD).

(C) The calculated permeability (K_p; mean ± SD). A nested t-test was performed to show the significant differences with p = 0.0003 for 80–100% PR vs. 15–30% PR explants passage. The sampling points in b and c are 0.5, 1, 1.5, 2, 2.5, 3.5, 4.5, 20, 22, and 24 h. See Figure S4.

Previously in guinea pigs, collagenase I was used to partially digest the RWM *in vivo* and to increase its permeability.[21] Following this study, we tested the passage of DexF in the presence of 80 mg/mL collagenase I (Figure 6A). After 5 h of collagenase I treatment, we observed a sudden significant increase in the permeability of DexF in comparison to the control explants using a multiple unpaired t-test. The calculated Kp values are shown in Figure 6B. Our interpretation of the effect of collagenase I treatment was that the collagenase creates gaps through the OE layer, and the molecules could more easily cross the RWM (Figure 6C).

Alternatively in guinea pigs,[20] saponin has been shown to permeabilize the RWM by selectively removing cholesterol and making ~10–100 nm holes in the membrane.[34–36] Therefore, we also tested the effects of RWM permeabilization via saponin on DexF permeability. We employed similar concentrations of saponin (130 μg/ml) as suggested by the previous study and up to 22 h of treatment (Figure 6D). However, we did not observe any increase in DexF permeability in the saponin-treated explants (n = 5 P0; Figures 6D and 6E). We further increased the saponin concentration by 3×, 10×, and 100× and tested it on the same explants. Out of 5 explants, only one showed an increase in DexF passage and one order of magnitude in the K_p (Figures 6D and 6E). We also verified the viability of the explant with the increased permeability and found a large decrease in the PR of its metabolic activity (down to 20%), implying that decreased cell viability was an additional factor that explained the increased permeability.

DISCUSSION

In this study, we investigate the characteristics of the porcine RWM including its microstructure and the cellular constitution (Figure 1). The porcine RWM is found to have similar characteristics to the human RWM, including its uncanny resemblance in thickness. These data confirm that the porcine RWM can be a highly valuable model for studying drug delivery into the inner ear. Furthermore, our TEM investigation discovers the presence of cilia in the OE layer of the porcine RWM. To the best of our knowledge, no other study reports the presence of cilia in the OE layer of the RWM, and its presence or absence in humans needs to be confirmed. Given that cilia may have a role in propelling substances away from the RWM or participate in active transport, their presence can greatly affect the passage of molecules through the RWM.

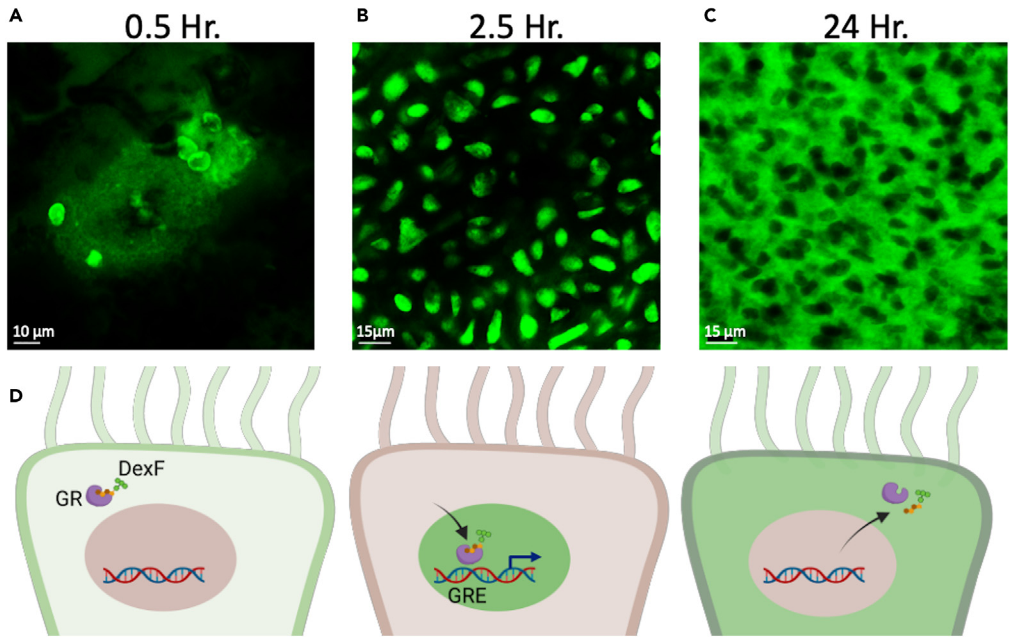

Figure 5. The porcine *ex vivo* model elucidates the interaction with and transport mechanism of dexamethasone-fluorescein into the RWM cells over time

(A) In confocal images after 0.5 h, only a few cell nuclei express fluorescence signal, and some low-intensity signal is present in the cytoplasm.

(B) After 2.5 h, the majority of the cell's nuclei express a strong fluorescence signal.

(C) After 24 h, the strong fluorescence signal is expressed in the cell cytoplasm, not in the nucleus.

(D) The schematic illustrates the migration of DexF into and out of the nucleus of OE cells. All the presented images are from fixed tissue. See Figures S5 and S6. GR: Glucocorticoid receptor, GRE: Glucocorticoid responsive element.

We have created an easy-to-fabricate and viable RWM chamber that can be utilized to measure the permeability of substances and to test diverse manipulation techniques to improve drug delivery to the inner ear. To test the functionality of this chamber, we employ Dex (Figure 2). The permeability value that is reported in the literature for *in vivo* testing of Dex in guinea pigs is 15 e−8 m/s.[33] The permeability value measured in our chamber (12.3 ± 4.6 e−8 m/s, n = 6) is very similar to that in *in vivo* testing procedures. Since the middle ear removal processes that exist in the *in vivo* experiment are absent in this chamber, Dex should continue to accumulate in the bottom chamber until it reaches equilibrium even until the second day. There are differences in the permeability value for Dex between the first and second days (p value: 0.0326), but there are no significant differences between 22 and 24 h statistically using nested t-test. It is worth mentioning that we measured permeability values cumulatively. In other words, the permeability value at a specific time point was calculated based on the total substance that had passed through the membrane up to that point. This approach has been used by other researchers previously.[23] However, this cumulative approach does not account for changes in the driving force gradient at any specific time. Alternatively, other studies have used instant permeability, where the amount of substance passage at any time point is measured as the difference between the current and previous sampling points.[37] This approach provides information on the temporal changes in the driving force as a function of time.

We have studied the passage of low-permeability DexF. Based on the literature, the passage of 1 mM DexF through the guinea pig RWM in 20–40 min is about 0.05–0.5 µg/mL.[20] Our measured passage values in 0.5 h for ∼500 µg/mL (0.5 mM) DexF using the porcine *ex vivo* RWM chamber is 0.16 ± 0.1 µg/mL and 0.02 ± 0.02 µg/mL for P0-20 (n = 6) and P40 (n = 3) RWM models, respectively. Once more, our measured value is strikingly close to what is reported in the literature using *in vivo* measurements. We also observed a significant decrease in the K_p of the P40 in comparison to P0-20 explants after 1 h, using a two-way ANOVA test (p value: 0.0121). This indicates an age effect on the permeability of the RWM, which could be due to the observed thickness difference of the RWM between P0 and P40 pigs. In most of the passage measurements, we observed a decrease in permeability over time. We can only speculate why we observe a

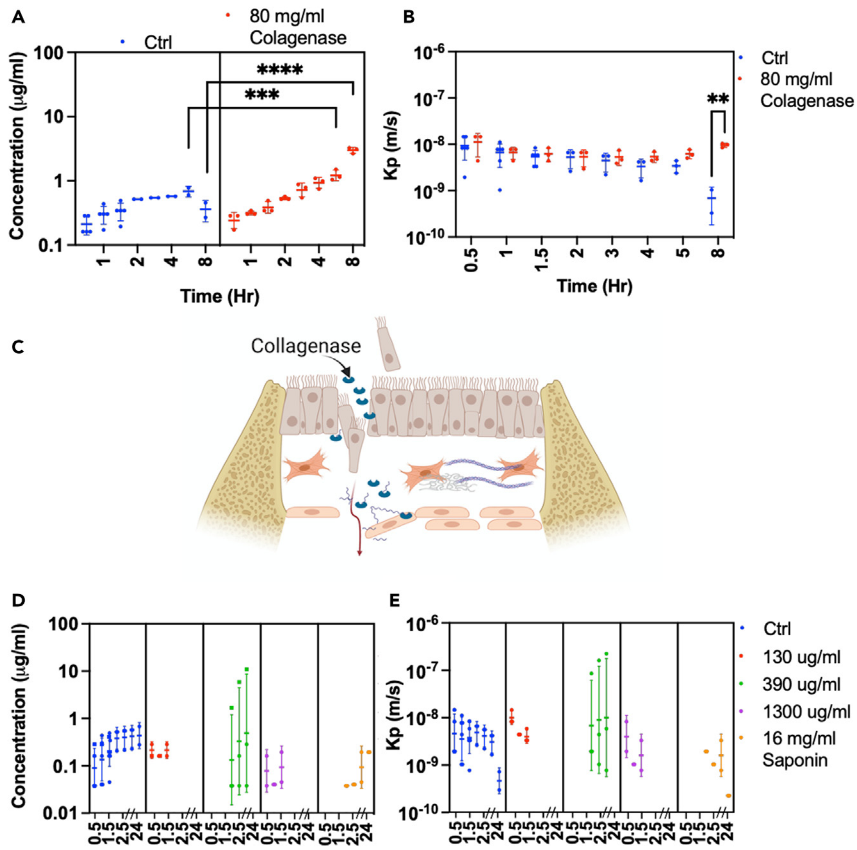

Figure 6. Collagenase I treatment enhanced the RWM permeability while saponin did not

(A) DexF ~500 µg/mL (0.5 mM) passage through the P0-P20 RWM chamber with (blue) and without (red) collagenase I treatment (80 mg/mL; n = 4; mean ± SD). After 5 h of collagenase I treatment, a significant increase in DexF passage was observed using a mixed-effect analysis (p value = 0.0021).

(B) The corresponding calculated permeability, K_p (mean ± SD), showed an increase in permeability after 8 h as well using a mixed-effect analysis (p value = 0.0081). The sampling points in a and b are 0.5, 1, 1.5, 2, 3, 4, 5, and 8 h hours.

(C) The schematic depicts the effect of collagenase treatment on the RWM structure and therefore RWM permeability.

(D) DexF ~500 µg/mL (0.5 mM) passage through the P0-P20 RWM chamber with and without saponin treatment at various concentrations of 130 µg/mL, 390 µg/mL, 1300 µg/mL, and 16 mg/mL. The DexF passage did not change after saponin treatment (n = 5, P20; mean ± SD).

(E) The corresponding calculated permeability, K_p (mean ± SD). The sampling points in d and e are 0.5, 1, 1.5, 2, 2.5, 3.5, and 24 h hours.

decrease in permeability over time. One of the possible reasons might be the aggregation of the DexF over time.

An advantage of the proposed RWM chamber is its ability to measure and track therapeutic substance passage over time. Consequently, the RWM chamber can serve as a platform to test new methods to enhance permeability, such as the conjugation of therapeutics with aptamers or peptides. New constructs could be tested and tuned using our proposed chamber similar to the approach taken to improve drug passage through the tympanic membrane.[38]

We also presented data from low-viable explants (15–30% PR) that are dying and showed that DexF passage through these explants is almost comparable to leaky, but healthy, explants (Figure 4). This is an important consideration that has been overlooked previously in other RWM models. Interestingly, in the low-viability and leaky explants, the passage pattern can be fitted with a logarithmic function suggesting that, in less-viable and leaky explants, diffusion is the main mechanism of passage rather than active passage mechanisms. This trend is similar to what is reported in the Kelso et al., 2015 study, where the micro-perforations created in the explant led to a faster diffusion. Here we employed the alamarBlue metabolic activity test as a reference for the level of cellular health of RWM explants (Figure 2). Metabolic activity tests have been previously used to examine the level of porcine *ex vivo* tissue activity.[39] In this respect, we cannot compare our results to a recent study that used human cadaveric RWM that went through freeze-thaw cycles.[37] Although their data similarly confirmed that the number of freeze-thaw cycles significantly increases the permeability of the tympanic membrane. Future studies will focus on improving the viability of the RWM explants beyond 3–5 days.

After establishing that the chamber shows a relative reduction in the passage of DexF compared to Dex, we demonstrated the enhanced passage of DexF using collagenase I treatment (Figure 6). However, collagenase I treatment required 5 h to significantly increase the passage of DexF. This treatment length is quite long when compared to the 0.5 h used with *in vivo* experiments on guinea pigs.[21] Also, on our hands, and in contrast with the literature,[20] porcine RWM permeabilization using saponin did not improve DexF permeability. These results could be explained due to the differences between the animal models. The RWM thickness in guinea pigs is reported to be 10–14 μm,[26] which is 5-6× thinner than the porcine and human RWM thickness.

In the future, we would like to use this RWM chamber to study the real-time passage of individual substances using high-resolution microscopy. Figure 5 shows an example of the use of the chamber for this purpose. We were able to observe that the fluorescence moves from the cytoplasm to the nucleus and back over a period of 24 h (Figure 5D). According to the literature, in the absence of a ligand, the glucocorticoid receptors–which are the target of Dex—stay in the cellular cytoplasm. In the event of binding to the ligand, these receptors translocate into the nucleus.[40] This phenomenon is similar to what we observed in the first 2.5 h of the passage of DexF, indicating that DexF binds to the receptor and the complex moves to the nucleus. Inside the nucleus, it is reported that these receptors bind to the responsive elements in the promoter regions of the target genes[40]; where the interaction of glucocorticoid receptors and responsive elements is dynamic to upregulate their steady-state association with their responsive gene promoters. After modulating the transcription of responsive genes, the receptor dissociates from the ligand and returns to the cytoplasm.[40] This can explain the fluorescence reappearing in the cytoplasm after 24 h (Figure 5C).

Our following objective is to compare the RWM chamber measurements with *in vivo* experiments in pigs. As a first step, we developed techniques to deliver substances including DexF and trypan blue via intratympanic injection in cadaver pigs (Figure S6). The developed surgical technique opens up opportunities for *in vivo* experiments.

Limitations of the study

This study has some limitations that will be addressed in the future. First, our yield of producing a non-leaking RWM chamber is only ∼50%. In our hands, the younger the animal from which the RWM has been extracted, the higher the success rate. In our experiments, this is not a limiting factor as producing chambers is relatively fast and we have ample access to fresh pig cadavers. In the future, we plan to improve the yield of the process. Second, we were only able to maintain the RWM cells in good health for 5 days. This provides a narrow window to perform the experiments. In the future, we plan to optimize the cell-culturing conditions and maintain the RWM chamber viability for a longer period. Another limitation is that, in our experiments, Dex is dissolved in methanol. Methanol is cytotoxic and could lead to changes in the measured RWM permeability. In the future, we plan to either use a more biocompatible solvent or use hydrogels to ameliorate the low solubility limit of Dex.

We expect to measure slightly higher permeability values in our *ex vivo* model relative to *in vivo* measurements. We believe this is the case since the *ex vivo* model does not account for additional removal mechanisms that exist in the middle and inner ear.[33,41,42] Nevertheless, the measured permeability values confirm the functionality of our *ex vivo* RWM chamber.

STAR★METHODS

Detailed methods are provided in the online version of this paper and include the following:

- KEY RESOURCES TABLE
- RESOURCE AVAILABILITY
  - Lead contact
  - Materials availability

SUPPLEMENTAL INFORMATION

Supplemental information can be found online at https://doi.org/10.1016/j.isci.2023.106789.

ACKNOWLEDGMENTS

The authors would like to thank the NCSU Central Procedure Lab for their help with tissue collection. We also want to thank NCSU Swine Education Unit (SEU) for their donation of animal carcasses. The authors would like to thank Dr. Jaewook Chung and Shohan Shohanuzzaman for their help with viability measurements as well as Kristen Popowski and Dr. Kathryn Polkoff with their help with media formulation. The initial data for this study were generated using the CMI-Young Scholar Program (YSP) seed grant. Research reported in this publication was supported by NIDCD of the National Institutes of Health under award numbers K99DC019960 (AM), R21DC020005 (AG), and R01DC021110 (AGC). We would like to thank the course directors (Ruth Anne Eatock, Andy Groves, Philip Joris, and Bradley Walters) and teaching assistants at the Biology of the Inner Ear 2022 course at the Marine Biological Laboratory (MBL)- University of Chicago. We would also like to thank Louis Kerr and the central microscopy facility at MBL. Some figures were generated during the Biology of the Inner Ear 2022 course. This work was performed in part at the Analytical Instrumentation Facility (AIF) at North Carolina State University, which is supported by the State of North Carolina and the National Science Foundation (award number ECCS-2025064). The AIF is a member of the North Carolina Research Triangle Nanotechnology Network (RTNN), a site in the National Nanotechnology Coordinated Infrastructure (NNCI).

AUTHOR CONTRIBUTIONS

Conceptualization: AM, AG, FSL; Methodology: AM, AG; Investigation: AM, DS, TM, KA; Visualization: AM; Resources: AM, AG; Supervision: AM, AG, FSL, AC; Writing—original draft: AM; Writing—review & editing: AM, AG, FSL, AC, DF, CZ, KAH.

DECLARATION OF INTERESTS

The authors declare no competing interests. The authors have assigned rights to a pending patent application to North Carolina State University.

INCLUSION AND DIVERSITY

We worked to ensure sex balance in the selection of non-human subjects. One or more of the authors of this paper self-identifies as a gender minority in their field of research. One or more of the authors of this paper self-identifies as living with a disability. While citing references scientifically relevant for this work, we also actively worked to promote gender balance in our reference list. We avoided "helicopter science" practices by including the participating local contributors from the region where we conducted the research as authors on the paper.

Received: September 26, 2022
Revised: March 16, 2023
Accepted: April 26, 2023
Published: May 2, 2023

REFERENCES

1. World Health Organization Deafness and Hearing Loss. Deafness and hearing loss. https://www.who.int/news-room/fact-sheets/detail/deafness-and-hearing-loss.
2. Livingston, G., Huntley, J., Sommerlad, A., Ames, D., Ballard, C., Banerjee, S., Brayne, C., Burns, A., Cohen-Mansfield, J., Cooper, C., et al. (2020). Dementia prevention, intervention, and care: 2020 report of the Lancet Commission. Lancet *396*, 413–446. https://doi.org/10.1016/S0140-6736(20)30367-6.
3. Nadhimi, Y., and Llano, D.A. (2021). Does hearing loss lead to dementia? A review of the literature. Hear. Res. *402*, 108038. https://doi.org/10.1016/j.heares.2020.108038.
4. Shulman, A., Goldstein, B., and Strashun, A.M. (2009). Final common pathway for tinnitus: theoretical and clinical implications of neuroanatomical substrates. Int. Tinnitus J. *15*, 5–50.
5. Camarena, A., Manchala, G., Papadopoulos, J., O'Connell, S.R., and Goldsworthy, R.L. (2021). Pleasantness ratings of musical dyads in cochlear implant users. Brain Sci. *12*, 33. https://doi.org/10.3390/brainsci12010033.
6. Goldsworthy, R.L., and Markle, K.L. (2019). Pediatric hearing loss and speech recognition in quiet and in different types of background noise. J. Speech Lang. Hear. Res. *62*, 758–767. https://doi.org/10.1044/2018_JSLHR-H-17-0389.
7. Lesica, N.A. (2018). Why do hearing aids fail to restore normal auditory perception? Trends Neurosci. *41*, 174–185. https://doi.org/10.1016/j.tins.2018.01.008.
8. Blanc, F., Mondain, M., Bemelmans, A.-P., Affortit, C., Puel, J.-L., and Wang, J. (2020). rAAV-mediated cochlear gene therapy: prospects and challenges for clinical application. J. Clin. Med. *9*, 589. https://doi.org/10.3390/jcm9020589.
9. Anderson, C.R., Xie, C., Su, M.P., Garcia, M., Blackshaw, H., and Schilder, A.G.M. (2019). Local delivery of therapeutics to the inner ear: the state of the science. Front. Cell. Neurosci. *13*, 418.
10. Rybak, L.P., Dhukhwa, A., Mukherjea, D., and Ramkumar, V. (2019). Local drug delivery for prevention of hearing loss. Front. Cell. Neurosci. *13*, 300. https://doi.org/10.3389/fncel.2019.00300.
11. Barrs, D.M., Keyser, J.S., Stallworth, C., and McElveen, J.T. (2001). Intratympanic steroid injections for intractable ménière's disease. Laryngoscope *111*, 2100–2104. https://doi.org/10.1097/00005537-200112000-00003.
12. Bird, P.A., Begg, E.J., Zhang, M., Keast, A.T., Murray, D.P., and Balkany, T.J. (2007). Intratympanic versus intravenous delivery of methylprednisolone to cochlear perilymph. Otol. Neurotol. *28*, 1124–1130. https://doi.org/10.1097/MAO.0b013e31815aee21.
13. de Cates, C., and Winters, R. (2022). Intratympanic steroid injection. In StatPearls (StatPearls Publishing).
14. Rauch, S.D., Halpin, C.F., Antonelli, P.J., Babu, S., Carey, J.P., Gantz, B.J., Goebel, J.A., Hammerschlag, P.E., Harris, J.P., Isaacson, B., et al. (2011). Oral vs intratympanic corticosteroid therapy for idiopathic sudden sensorineural hearing loss: a randomized trial. JAMA *305*, 2071–2079. https://doi.org/10.1001/jama.2011.679.
15. Schoo, D.P., Tan, G.X., Ehrenburg, M.R., Pross, S.E., Ward, B.K., and Carey, J.P. (2017). Intratympanic (IT) therapies for menière's disease: some consensus among the confusion. Curr. Otorhinolaryngol. Rep. *5*, 132–141. https://doi.org/10.1007/s40136-017-0153-5.
16. Seidman, M.D., and Vivek, P. (2004). Intratympanic treatment of hearing loss with novel and traditional agents. Otolaryngol. Clin. *37*, 973–990.
17. Tang, B., Jia, Y., Shi, Z., Shen, Y., Li, D., Huang, H., Yang, B., Wang, D., and Feng, Q. (2018). Intratympanic injection of dexamethasone after failure of intravenous prednisolone in simultaneous bilateral sudden sensorineural hearing loss. Am. J. Otolaryngol. *39*, 676–678. https://doi.org/10.1016/j.amjoto.2018.07.008.
18. Goycoolea, M.V. (2001). Clinical aspects of round window membrane permeability under normal and pathological conditions. Acta Otolaryngol. *121*, 437–447. https://doi.org/10.1080/000164801300366552.
19. Arriaga, M., Arteaga, D.N., Fafalis, D., Yu, M., Wang, X., Kasza, K.E., Lalwani, A.K., and Kysar, J.W. (2021). Membrane curvature and connective fiber alignment in Guinea pig round window membrane. Acta Biomater. *136*, 343–362. https://doi.org/10.1016/j.actbio.2021.09.036.
20. Li, W., Hartsock, J.J., Dai, C., and Salt, A.N. (2018). Permeation enhancers for intratympanically-applied drugs studied using fluorescent dexamethasone as a marker. Otol. Neurotol. *39*, 639–647. https://doi.org/10.1097/MAO.0000000000001786.
21. Wang, H., Murphy, R., Taaffe, D., Yin, S., Xia, L., Hauswirth, W.W., Bance, M., Robertson, G.S., and Wang, J. (2012). Efficient cochlear gene transfection in Guinea-pigs with adeno-associated viral vectors by partial digestion of round window membrane. Gene Ther. *19*, 255–263. https://doi.org/10.1038/gt.2011.91.
22. Lin, Y.-C., Shih, C.-P., Chen, H.-C., Chou, Y.-L., Sytwu, H.-K., Fang, M.-C., Lin, Y.-Y., Kuo, C.-Y., Su, H.-H., Hung, C.-L., et al. (2021). Ultrasound microbubble–facilitated inner ear delivery of Gold nanoparticles involves transient disruption of the tight junction barrier in the round window membrane. Front. Pharmacol. *12*, 689032.
23. Kelso, C.M., Watanabe, H., Wazen, J.M., Bucher, T., Qian, Z.J., Olson, E.S., Kysar, J.W., and Lalwani, A.K. (2015). Microperforations significantly enhance diffusion across round window membrane. Otol. Neurotol. *36*, 694–700. https://doi.org/10.1097/MAO.0000000000000629.
24. Glueckert, R., Johnson Chacko, L., Rask-Andersen, H., Liu, W., Handschuh, S., and Schrott-Fischer, A. (2018). Anatomical basis of drug delivery to the inner ear. Hear. Res. *368*, 10–27. https://doi.org/10.1016/j.heares.2018.06.017.
25. Goycoolea, M.V., and Lundman, L. (1997). Round window membrane. Structure function and permeability: a review. Microsc. Res. Tech. *36*, 201–211. https://doi.org/10.1002/(SICI)1097-0029(19970201)36:3<201::AID-JEMT8>3.0.CO;2-R.
26. Goycoolea, M.V., Carpenter, A.M., and Muchow, D. (1987). Ultrastructural studies of the round-window membrane of the cat. Arch. Otolaryngol. Head Neck Surg. *113*, 617–624.
27. Nordang, L., Linder, B., and Anniko, M. (2003). Morphologic changes in round window membrane after topical hydrocortisone and dexamethasone treatment. Otol. Neurotol. *24*, 339–343.
28. Schachern, P.A., Paparella, M.M., and Duvall, A.J. (1982). The normal chinchilla round window membrane. Arch. Otolaryngol. *108*, 550–554.
29. Lundman, L., Bagger-Sjöbäck, D., Holmquist, L., and Juhn, S. (1987). Round window membrane permeability. An in vitro model. Acta Otolaryngol. Suppl. *442*, 41–43. https://doi.org/10.3109/00016488709102837.
30. Sun, J.j., Liu, Y., Kong, W.j., Jiang, P., and Jiang, W. (2007). In vitropermeability of round window membrane to transforming dexamethasone with delivery vehicles — a dosage estimation. Chin. Med. J. *120*, 2284–2289.
31. Witte, M.C., and Kasperbauer, J.L. (2000). Round window membrane permeability to transforming growth factor-α: an in vitro study. Otolaryngol. Head Neck Surg. *123*, 91–96. https://doi.org/10.1067/mhn.2000.106006.
32. Moatti, A., Cai, Y., Li, C., Sattler, T., Edwards, L., Piedrahita, J., Ligler, F.S., and Greenbaum, A. (2020). Three-dimensional imaging of intact porcine cochlea using tissue clearing and custom-built light-sheet microscopy. Biomed. Opt Express *11*, 6181–6196. https://doi.org/10.1364/BOE.402991.
33. Salt, A.N., Hartsock, J.J., Piu, F., and Hou, J. (2018). Dexamethasone and dexamethasone-phosphate entry into perilymph compared for middle ear applications in Guinea pigs. Audiol. Neurootol. *23*, 245–257. https://doi.org/10.1159/000493846.
34. Chen, M., Balhara, V., Jaimes Castillo, A.M., Balsevich, J., and Johnston, L.J. (2017). Interaction of saponin 1688 with phase separated lipid bilayers. Biochim. Biophys. Acta, Biomembr. *1859*, 1263–1272. https://doi.org/10.1016/j.bbamem.2017.03.024.

35. Keukens, E.A., de Vrije, T., van den Boom, C., de Waard, P., Plasman, H.H., Thiel, F., Chupin, V., Jongen, W.M., and de Kruijff, B. (1995). Molecular basis of glycoalkaloid induced membrane disruption. Biochim. Biophys. Acta *1240*, 216–228. https://doi.org/10.1016/0005-2736(95)00186-7.

36. Seeman, P., Cheng, D., and Iles, G.H. (1973). Structure of membrane holes in osmotic and saponin hemolysis. J. Cell Biol. *56*, 519–527. https://doi.org/10.1083/jcb.56.2.519.

37. Veit, J.G.S., Birru, B., Wang, Y., Singh, R., Arrigali, E.M., Park, R., Miller, B., Firpo, M.A., Park, A.H., and Serban, M.A. (2022). An evaluation of the drug permeability properties of human cadaveric in situ tympanic and round window membranes. Pharmaceuticals *15*, 1037. https://doi.org/10.3390/ph15091037.

38. Kurabi, A., Schaerer, D., Noack, V., Bernhardt, M., Pak, K., Alexander, T., Husseman, J., Nguyen, Q., Harris, J.P., and Ryan, A.F. (2018). Active transport of peptides across the intact human tympanic membrane. Sci. Rep. *8*, 11815. https://doi.org/10.1038/s41598-018-30031-6.

39. Erickson-DiRenzo, E., Sivasankar, M.P., and Thibeault, S.L. (2015). Utility of cell viability assays for use with ex vivo vocal fold epithelial tissue. Laryngoscope *125*, E180–E185. https://doi.org/10.1002/lary.25100.

40. Nicolaides, N.C., Chrousos, G., and Kino, T. (2000). Glucocorticoid receptor. In Endotext, K.R. Feingold, B. Anawalt, A. Boyce, G. Chrousos, W.W. de Herder, K. Dhatariya, K. Dungan, J.M. Hershman, J. Hofland, and S. Kalra, et al., eds. (MDText.com, Inc.).

41. Lim, D.J., and Hussl, B. (1975). Macromolecular transport by the middle ear and its lymphatic system. Acta Otolaryngol. *80*, 19–31. https://doi.org/10.3109/00016487509121296.

42. McLean, W.J., Hinton, A.S., Herby, J.T.J., Salt, A.N., Hartsock, J.J., Wilson, S., Lucchino, D.L., Lenarz, T., Warnecke, A., Prenzler, N., et al. (2021). Improved speech intelligibility in subjects with stable sensorineural hearing loss following intratympanic dosing of FX-322 in a phase 1b study. Otol. Neurotol. *42*, e849–e857. https://doi.org/10.1097/MAO.0000000000003120.

STAR★METHODS

KEY RESOURCES TABLE

REAGENT or RESOURCE	SOURCE	IDENTIFIER
Antibodies		
Anit-EpCAM, CD326	Abcam	ab71916; RRID:AB_1603782
Anti-Vimentin	Santa Cruz Biotechnology	sc-6260; RRID:AB_628437
Goat anti-mouse AF 647	Thermofisher Invitrogen	A21236; RRID:AB_2535805
Goat anti-rabbit AF 488	Thermofisher Invitrogen	A11008; RRID:AB_143165
Biological samples		
Porcine round window membrane explant	NCSU-swine education unit	Yorkshire
Critical commercial assays		
Competitive Dexamethasone ELISA kit, 0.1 ppb sensitivity	MyBioSource	MBS2548580
Experimental models: Organisms/strains		
Porcine	NCSU-swine education unit	Yorkshire
Software and algorithms		
Prism 9.2	graphpad	https://www.graphpad.com/scientific-software/prism/
Biorender	Web application	https://biorender.com/
Other		
Dako	Agilent	X0909
Pro-Long Gold	Thermofisher Invitrogen	P36930
sodium cacodylate buffer	Clini Sciences	11652
EMbed-812	Electron microscopy sciences	50-980-391
Dulbecco's Modified Eagle Medium (DMEM)	Corning Life Sciences	10-013-CM
fetal bovine serum	Cytiva	SH30396.03
antibiotic-antimycotic	Sigma-Aldrich	A5955-20 ML
N2	Thermofisher	17502048
AlamarBlue cell viability reagent	Thermofisher	DAL1025
Dental cement	3M RelyX Unicem,	56830
Dexamethasone	Thermofisher	D1383
Dexamethasone-fluorescein	Sigma	D4902
Saponin	Sigma	47036
DAPI	Sigma	D9542
NucBlue	Fisher Scientific	R37606
Collagenase type I	Sigma	SCR103

RESOURCE AVAILABILITY

Lead contact

Further information and requests for resources and reagents should be directed to and will be fulfilled by the lead contact, Alon Greenbaum (greenbaum@ncsu.edu).

Materials availability

This study did not generate new unique reagents.

Data and code availability

The data used in this study is available from the lead contact upon reasonable request.

The software that was used in this study is listed in the key resources table.

Any additional information required to reanalyze the data reported in this study is available from the lead contact upon reasonable request.

EXPERIMENTAL MODEL AND SUBJECT DETAILS

In this study, we utilized 23 Yorkshire wild-type pigs (both sexes) on postnatal days 0: P0, P20, and P40. All animal protocols were approved by the Institutional Animal Care and Use Committee (IACUC) at North Carolina State University, following the standards of the National Institute of Health and Committee on Care and Use of Laboratory Animals.

METHOD DETAILS

Dissection and chamber fabrication

First, we removed the skin and created a large window on top of the porcine skull using a bone stryker.[32] The brain was discarded to observe the inner ear. Then, we cut further into the bone surrounding the inner ear via the stryker and excised the porcine inner ear using a bone cutter. Taking the inner ear out of the bony environment requires care to maintain the RWM intact. Using a dental drill and 1 mm drill bit, we excised the RWM including a small portion of the surrounding bone (Figure S2). The whole drilling procedure was done inside a fresh PBS solution including 1% Antibiotic/Antimycotic, which was routinely exchanged to minimize the accumulation of debris. After the excision, the surrounding bone around the RWM was dried out using sterile gauze pads and glued into the bottom of a cut 0.5 mm Eppendorf tube using dental cement (3M RelyX Unicem, 56830) as shown in Figure S2. The glued RWM was then mounted on top of a Transwell without the mesh and immersed in cell culture media (DMEM, 1% Antibiotic/Antimycotic, 1% N2) overnight (150 μl on top of the RWM and 1.5 ml on the bottom). The next morning the media was changed (DMEM, 1% FBS, 1% Antibiotic/Antimycotic, 1% N2) and the chamber was ready for experimental work.

Exclusion criteria to detect leaky or unhealthy RWM chambers

- If tears or holes in the RWM were observed visually using a dissecting microscope.
- If the membrane lost more than 100 μL of media overnight, this normally indicates the presence of micron size holes in the RWM that cannot be observed using a dissecting microscope.
- If the viability test was below 80% PR at the beginning of the passage experiment.
- If the viability test was below 20% PR at the end of the passage experiment.

We start testing our samples when they were viable and healthy, i.e., when they showed a PR value of above 80%. We decided to measure RWM permeability only in chambers where the percent reduction–PR is at least 80% in order to exclude the impact of increasing cell mortality. We postulated that explants with lower PR i.e., ~60% might have a significant number of cells that are not viable, and therefore, their value might not reflect the in-vivo conditions. To support this claim, Figure 4 shows that chambers with 20% PR behave like leaky chambers.

We have also tested the passage of Trypan blue with this method,[38] and its passage can also be used as an exclusion criterion. Trypan blue is a big molecule therefore, non-leaky chambers should limit its passage. The Figure below shows Trypan blue passage in a non-leaky explant. The one-way ANOVA test shows no significance in the ratio of the passage over time. Whenever there was a loss of media from the leaky chamber, trypan blue was observed at the bottom of the chamber.

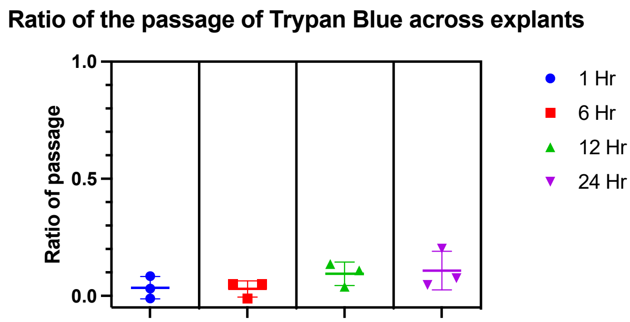

AlamarBlue viability test

To perform the viability test, first, the explants were washed with PBS three times. Then 1 ml of fresh media containing 10% alamarBlue (Thermofiher, Dal1025) was added to the chamber (top and bottom). The explants were placed in the incubator for 4–6 hours The plate that covered the chamber was removed and absorbance was measured using a plate reader (Infinite M Plex from Tecan) at two wavelengths (570 nm and 600 nm). The percent reduction was calculated based on the vendor's instructions.

Permeability measurements

To measure the permeability of substances, we mixed ~100 μl culture media (DMEM, 1% FBS, 1% Antibiotic Antimycotic, 1% N2) with the substance and placed the mixture in the top chamber. The top solution was redosed at the amount of 10 μl at each sampling (7–9 times) to meet the conditions of a continuous infinite dosing.[23] The bottom chamber was filled with 1.5 ml of cell culture media in a 24-well plate (for Dex, the bottom chamber was filled with 1 ml of the media). To monitor the progression of the passage, the media at the bottom of the chamber was sampled. In each sampling event, ~100 μl of liquid was withdrawn from the bottom of the chamber. Before sampling, the media was pipette up and down to mix and homogenize. After sampling the media, 100 μl fresh media was added to the bottom chamber, this dilution in the media was compensated when calculating the concentrations by considering the total volume as the original volume plus the withdrawn amounts.[30] The purpose of replacing the solution was to simulate the static cell diffusion condition.

The non-salt form of dexamethasone (Dex) (molecular weight: 392.46) was dissolved in methanol first to obtain a concentration of 10 mg/ml and diluted in the media to obtain a concentration of ~400 ug/ml or 1 mM. The Dex concentration may be above the solubility limit. Our solution was clear, but we cannot be absolutely sure if all the Dex was in solution. There might be small aggregates of suspended Dex or Dex may have adsorbed to the proteins in the culture media. The dexamethasone conjugated with fluorescein (DexF) (molecular weight: 840.98) was dissolved in methanol first to obtain 1 mg/ml and diluted in the media to obtain ~400 ug/ml or 0.5 mM, per the manufacturer's instructions.

Dexamethasone ELISA

We used a ready-to-use ELISA kit (Mybiosource, MBS2548580) for measuring Dex concentration in the media collected from the bottom chamber. To generate a standard curve, values of absorbance, which were acquired using a microplate reader (VERSA max), were correlated with known Dex concentrations (0.1–10 ppb). The concentration of Dex in liquid samples can be then calculated by comparing the OD of the samples to the standard curve. The standard fitting curve close to the OD values from the bottom chamber (0.6–1.3) was used to improve the accuracy. The Dex samples were diluted 40000x to be detected using this kit.

Immunostaining

The RWM tissue explants were fixed using 4% paraformaldehyde (PFA) and then permeabilized and blocked using IHC blocking buffer (serum-free protein block, Dako from Agilent, X0909) with 0.4% Triton for 1 hour at RT (room temperature). Explants were then stained against vimentin and EpCAM at a 1:100 dilution. Explants were incubated with primary antibodies overnight at 4°C. Then, the explants were washed with PBS and incubated with secondary antibodies at a 1:200 dilution for 1.5 hours at RT. For nuclear staining, two drops of NucBlue were added to each well after 30 minutes of secondary incubation. The cells were washed with PBS and mounted with ProLong Gold at RT for 4 hours before observation. Explants were imaged using an Olympus FLUOVIEW confocal microscope to detect nuclei, vimentin, and EpCAM. To quantify the RWM thickness, we used IMARIS software.

Transmission electron microscopy

For TEM investigation, the tissues were fixed using 4% PFA and 1% Glutaraldehyde in 0.1% sodium cacodylate at 4°C overnight. The tissues were washed 3x in 0.1 M sodium cacodylate buffer. The tissues were incubated with 2% osmium tetroxide for 1 hour. The tissues were washed 3x in 0.1 M sodium cacodylate buffer. Then, the tissues were dehydrated in 70% and 95% ETOH for 20–30 min at each step and 2x at 100% ETOH for 30 min. The tissues were incubated with 2:1 and 1:1 ethanol: resin solution, for 1 hour each. The tissues were incubated overnight in 1:1 ethanol: resin. The tissues were incubated with 1:2 ethanol: resin for 1 hour and with 100% EMbed-812 resin 2X for 1 hour each. The tissues were transferred to pure resin and incubated at 70 C overnight for resin embedding. Ultramicrotomy (Leica UC7 ultramicrotome) was used to obtain 85 nm thick cross-sections. Lead citrate/ Uranyl acetate post staining of grids was performed. We have used the Bio-TEM model HT7800-120 kV transmission electron microscope for imaging.

QUANTIFICATION AND STATISTICAL ANALYSIS

The permeability coefficient (K_P) calculation

The permeability coefficient (K_P) in m/s was calculated using the following formula[23]:

$$K_p = \frac{Q}{A \cdot t \cdot (C_T - C_B)}$$

Where Q is the mass in μg of substance transported through the RWM in time (t) in seconds across the RWM area (A) in m^2. The C_T and C_B are the concentrations in μg/ml on the top and bottom of the RWM. The (C_T-C_B) is considered equal to C_T under redosing conditions since C_T is considerably higher than C_B.

We used one-way ANOVA, to investigate the significant differences in K_p between ages using GraphPad Prism version 9.5. A multiple unpaired t-test was used to investigate the effect of RWM permeabilization on the passage difference of DexF. The statistical details of experiments can be found in each figure caption.